Asymmetric Rolling Contact Joint for Enhanced Payload Capabilities

Jeongdo Ahn, Minho Hwang, Dukyoo Kong, Joonhwan Kim, and Dong-Soo Kwon, *Senior Member, IEEE*

***Abstract*—It is challenging for a surgical joint to tolerate a sufficient payload when downsizing its diameter. The trade-off between payload and diameter is even more evident when designing robots with strict size constraints, such as in flexible endoscopic surgery applications. To address this issue, we propose a novel asymmetric rolling contact (ARC) joint that has two different rolling radii with a wire hole slit that is actuated by a tendon-driven mechanism. The ARC joint is designed to tolerate a high payload in the dominant direction, such as when lifting tissue or pulling a suture thread. We analyzed the effects of various design variables on the payload capability of the ARC joint. The results of the payload experiment suggest that the designed ARC joint has a maximum payload of 2.6 N with a 3.4 mm diameter, which enhances the payload by 71.9% compared to the conventional symmetric rolling joint. We confirmed that the endoscopic surgical task may be feasibly conducted using the proposed joint for two major tasks: endoscopic submucosal dissection and surgical suturing.**

***Index Terms*—Flexible endoscopic surgery, high payload, rolling contact joint, surgical manipulator, tendon-driven mechanism.**

I. Introduction

GASTROINTESTINAL (GI) cancer occurs frequently and exhibited the second highest mortality rate according to the World Health Organization (WHO) in 2018 [1]. Statistics show that the early detection and treatment of GI cancer are crucial. Although standard endoscopy plays a significant role in the early detection and treatment of GI cancer [2], this system is designed for diagnosis and therefore has limitations when used to perform more advanced procedures [3]. The flexible instrument introduced in to the channel of the endoscope can only be rotated and translated. In addition, because the standard endoscope has one instrument channel, only a single instrument can be used for endoscopic procedures. The lack of adequate degrees of freedom (DOF) and low payload capabilities when using a single instrument severely limits this system. Because of the lack of tissue manipulation capabilities, it is not possible to achieve adequate counter traction for dissecting and ensuring proper endoscopic imaging [4], [5], which may result in bleeding or perforation during endoscopic procedures [6]. Moreover, suturing for wound closure, which is an essential task in advanced endoscopic surgery, is impossible because it requires at least two dexterous instruments [7]. Although various dedicated manual devices have been developed for suturing in flexible endoscopic procedures [8], [9], [10], [11], they have limitations in their applications toward flexible endoscopy, such as low dexterity, low adaptability to various wound sizes, and lack of applicability in other procedures.

Recently, to overcome the aforementioned limitations of conventional endoscopes, flexible endoscopic surgery robots for performing endoscopic surgery or for natural orifice transluminal endoscopic surgery (NOTES) by approaching narrow and curved intraluminal space have been developed, such as ViaCath [12], EndoMaster [13], [14], [15], FLEX [16], [17], i2Snake [18], [19], STRAS [20], [21], RAFE [22], and K-FLEX [23]. Most of these systems consist of a long and flexible overtube, with two flexible instruments deployed within the inner channel. The flexible instrument steers the end-effector using an articulation joint to create the dexterous motions required for tissue manipulation or suturing. In general, an articulation joint consists of two bending DOFs, namely yaw and pitch. In this article, yaw refers to the left and right bending movements and pitch refers to the up and down bending movements when viewing the surgical instrument from the frontal plane (axial direction). Furthermore, this joint should have a sufficient payload even with a small diameter for the purpose of lifting tissue during endoscopic submucosal dissection (ESD) [24] or pulling thread during suturing [25], [26]. However, the payload capability of a surgical joint decreases exponentially with the size of the joint. The payload of a joint is proportional to the following

Manuscript received 11 November 2022; revised 6 April 2023; accepted 30 April 2023. Date of publication 20 July 2023; date of current version 16 February 2024. Recommended by Technical Editor Q. Ahmed and Senior Editor W. J. C. Zhang. This work was supported in part by the International Joint Technology Development Project funded by the Korean Ministry of Trade, Industry, and Energy under Grant P0006718 and in part by the Technology Innovation Program under Grant 1415178694 of the Ministry of Trade, Industry and Energy, Korean Government. *(Corresponding author: Dong-Soo Kwon.)*

Jeongdo Ahn is with the Department of Robotics and Mechatronics, Korea Institute of Machinery and Materials, Daejeon 34103, South Korea (e-mail: jdahn@kimm.re.kr).

Minho Hwang is with the Department of Robotics and Mechatronics Engineering, Daegu Gyeongbuk Institute of Science & Technology, Daegu 42988, South Korea (e-mail: minho@dgist.ac.kr).

Dukyoo Kong and Joonhwan Kim are with the R&D Center of ROEN Surgical, Inc., Daejeon 34051, South Korea (e-mail: kongdy@roensurgical.com; te108715@gmail.com).

Dong-Soo Kwon is with the Department of Mechanical Engineering, Korea Advanced Institute of Science and Technology, Daejeon 34141, South Korea (e-mail: kwonds@kaist.ac.kr).

This article has supplementary material provided by the authors and color versions of one or more figures available at https://doi.org/10.1109/TMECH.2023.3279648.

Digital Object Identifier 10.1109/TMECH.2023.3279648

parameters: 1) size of the moment arm, that is, the diameter of the joint, and 2) the allowable tension of the actuation wire, that is, the size of the cross-sectional area of the actuation wire. As a result, as the diameter of the surgical joint and cross-sectional area of the actuation wire reduces, the payload of the joint reduces significantly. Owing to the tradeoff between payload and instrument diameter, downsizing the surgical joint while maintaining payload is a challenging issue for stable endoscopic surgery. Furthermore, the instrument payload during both the straightening and bending phases must be high. In this study, the straightening and bending phases describe straightening the joint from a bent posture and bending the joint from a straightened posture, respectively.

Attempts have been made to increase the payloads of surgical manipulators. Choi proposed an elbow pitch joint consisting of a rigid rod and a flexible leaf spring to achieve a high payload [27]. This joint is similar to the slider-crank mechanism. However, owing to the flexible leaf spring, the payload was enhanced with a small looseness error. The rigid rod created a large moment arm with respect to the pivot point, and this rod increased the payload of the instrument. The maximum payload of the joint was 10 N with a diameter of 8 mm. This instrument could not perform two bending motions, however, because the use of only one bending pivot point to achieve bidirectional bending is impossible. Similarly, the elbow joint mechanism developed by Hwang [28] deployed a slider-crank linkage to achieve a high torque transmission capability. The payload increased as the joint angle increased because of the effect of the moment arm. This joint, with a diameter of 7 mm, could lift a weight of more than 15 N. However, as found by Choi [27], this joint was limited as only one bending motion and unilateral bending were possible. Furthermore, the rigid slider-crank limited the applicability of this system to flexible surgical instruments. A constrained continuum joint with a small diameter (3.7 mm) was also previously developed that exhibited a maximum payload of 3 N [29]. This joint structure enhanced the payload by constraining the redundancy of the continuum using auxiliary links. However, it is difficult to implement multibending DOFs in this structure, and the payload achieved in a straightened posture is relatively low.

Currently, no surgical joints have been made that are capable of two-DOF bending motions, can tolerate a high payload in both straightening and bending phases, and are flexible for applications in GI procedures. The symmetric structure of a surgical joint allows it to exert the same amount of force in both the yaw (upward and downward) and pitch (leftward and rightward) directions around the neutral axis. However, the payload required for endoscopic tasks is asymmetric. For example, ESD mainly requires a payload in the upward direction during endoscopy for countertraction of the tissue rather than in the downward direction [5] [see Fig. 1(a)]. In addition, knot tying during the suturing task requires exerting an outward force during thread pulling [see Fig. 1(b)].

In this study, we define the dominant direction as the direction requiring a high payload, as shown in Fig. 1(c) in case of right instrument. The dominant direction comprises straightening and bending phases, as shown in Fig. 2, which shows the side view

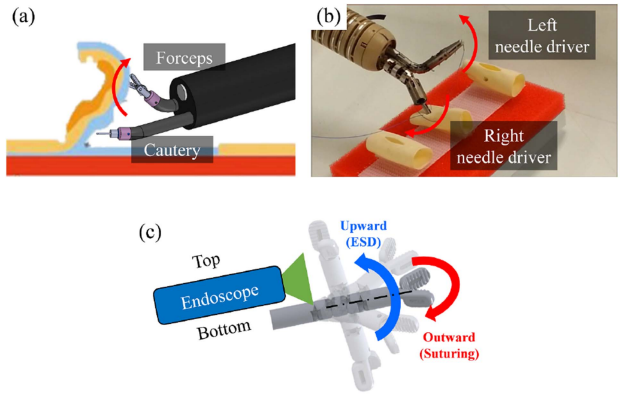

Fig. 1. Depending on the task, the dominant direction of the required payload differs. (a) During the ESD, the high payload of the forceps is required to upwardly lift the tissue (blue arrow). (b) During knot tying, the high payload of needle driver is required in the outward direction to pull the thread tightly (red arrow). (c) Dominant direction of right surgical instrument for tissue lifting (upward, blue arrow) and knot-tying (outward, red arrow).

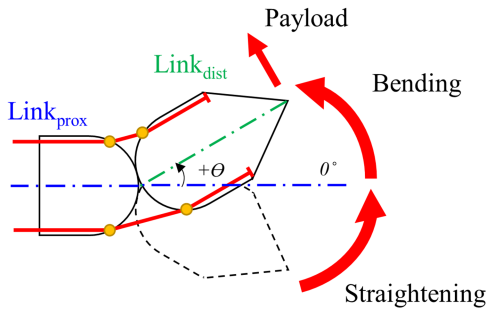

Fig. 2. Two phases of the bending motion of a joint depending on the sign of the bending angle (θ). The straightening phase corresponds to when the bending angle of the surgical instrument changes from a negative value to 0°. The bending phase corresponds to when the bending angle changes from 0° to a positive value.

of the 1-DOF joint. The blue and green dashed and dotted lines represent the neutral axes of the proximal and distal link, respectively. Because this joint has 1 DOF, these neutral axes should be on the paper plane. The bending angle (θ) is defined as the angle between the proximal neutral axis and distal neutral axis. Then, the positive bending angle is defined as the angle generated when the neutral axis of $Link_{dist}$ is moved from the neutral axis of $Link_{prox}$ in the dominant direction (high payload required direction). Therefore, the bending phase changes from zero to the bending angle (negative and positive angle), and the straightening phase returns to the zero state.

The goal of this study is to develop a steerable joint with a high payload in the dominant direction. We propose a novel joint design to enhance the payload in the dominant direction during both the straightening and bending phases (see Fig. 3). This joint has two different radii of the rolling surfaces. The rolling surface is a round-shaped surface, in which rolling occurs at joints where the adjacent links are in contact. When a joint bends, the two adjacent links roll on this rolling surface. In addition, the slit of the wire hole is designed to increase the

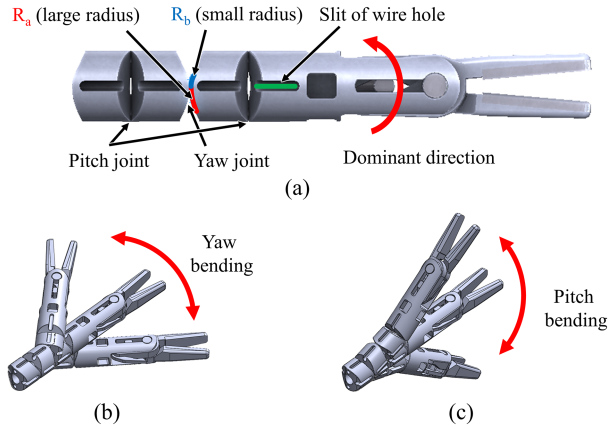

Fig. 3. Two-DOF surgical instrument with an ARC joint. The red and blue curved lines represent the large and small radii of the rolling surface, respectively. The straight green line represents the slit of the wire hole. The dominant direction of this instrument is upwards (red arrow).

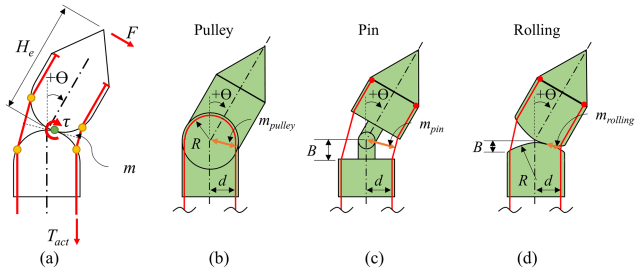

Fig. 4. (a) Schematic diagram for the payload calculation of a single joint. Simple kinematic structures of conventional symmetric joints: (b) pulley, (c) pin, and (d) rolling contact joint.

payload during the bending phase while maintaining the payload during the straightening phase. Moreover, this joint is capable of two-DOF bending because it can alternate yaw and pitch, similar to conventional joints.

The rest of this article is organized as follows. Compared to the conventional symmetric rolling contact joint, Section II describes the design process of the proposed asymmetric rolling contact (ARC) joint in terms of the payload. The payload capability of a real ARC joint is verified in Section III with two major endoscopic surgical tasks, ESD and suturing. The discussion for the experimental results is presented in Section IV. Finally, V concludes this article.

In summary, the contributions of this study can be listed as follows:

1) Novel joint design to tolerate a high payload in the dominant direction.
2) Establishment of a process for designing an ARC joint.
3) Verification of the high payload capability of the proposed ARC joint with a small diameter (payload: 2.6 N, diameter of instrument: 3.4 mm).
4) Verification of endoscopic surgical performance of this joint through two major tasks: a) ESD and b) suturing.

II. Design of ARC Joint

A. Payload Analysis of Symmetric Joint

The payload of a single joint is shown in Fig. 4(a). The two red lines on either side of the link represent the actuating wires. The end-tip payload of the surgical instrument can be calculated kinematically as

$$F = \frac{\tau}{H_e} = \frac{T_{\text{act}} m}{H_e} \tag{1}$$

where F is the payload generated at the end tip, τ is the torque at the joint, H_e is the length between the contact point of the joint and the end tip, T_{act} is the tension of the actuating wire, and m is the magnitude of the moment arm between the contact point of the joint and actuating wire. As per (1), the payload increases as the tension of the actuating wire and moment arm increases and the length of the end tip decreases. Owing to the limited actuating power or breaking load of the actuating wire, this tension may be limited. In addition, the length of the end tip is determined depending on the use of the surgical instrument. We next attempt to increase the magnitude of the moment arm, particularly in the dominant direction.

Fig. 4 also shows the simple kinematic structures of the pulley, pin, and rolling contact joints. When the bending angle is changed, the moment arm proportional to the payload may be calculated. For the pulley joint, the magnitudes of the left and right sides of the moment arm are always constant and equal to the pulley radius (R) or distance between the wire hole and central axis of the link (d) regardless of the bending angle

$$m_a(\theta) = m_b(\theta) = R = d \tag{2}$$

where the subscripts a and b denote the left- and right-sides, respectively. However, the magnitudes of the moment arms of the pin and rolling contact joints vary as the bending angle varies. When the pin joint is bent, the moment arm is calculated as

$$m_a(\theta) = d\cos\frac{\theta}{2} - B\sin\frac{\theta}{2} \tag{3}$$

$$m_b(\theta) = d\cos\frac{\theta}{2} + B\sin\frac{\theta}{2} \tag{4}$$

where B is the hole height. When the rolling contact joint is bent, the left- and right-side moment arms are calculated as

$$m_a(\theta) = d\cos\frac{\theta}{2} + (R-B)\sin\frac{\theta}{2} \tag{5}$$

$$m_b(\theta) = d\cos\frac{\theta}{2} - (R-B)\sin\frac{\theta}{2} \tag{6}$$

where R denotes the radius of the rolling surface. In the equations for the pin and rolling contact joints, the pin joint can be regarded as a rolling contact joint with a radius of zero for the rolling surface. To enhance the payload in the dominant direction, the moment arm on the right side $m_b(\theta)$ should be increased. Fig. 5 shows a comparison of the moment arms on the right side of each joint from a bending angle of $-50°$ to $50°$. Every joint had $d = 2$ mm such that their moment arms at $0°$ were equivalent. The heights of the wire holes of the pin and rolling contact joints were 2.5 mm. The radii of the rolling surface were set to 1.5 mm (red solid line), 3 mm (green solid line), and 4.5 mm

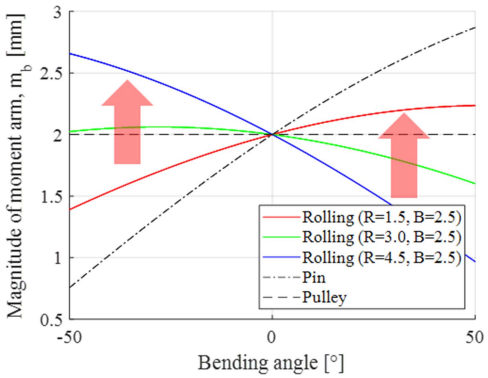

Fig. 5. Comparison of the magnitude of moment arms of conventional symmetric joints in the dominant direction (right-side). Dashed line = pulley joint; dashed and dotted line = pin joint; solid lines = rolling contact joints.

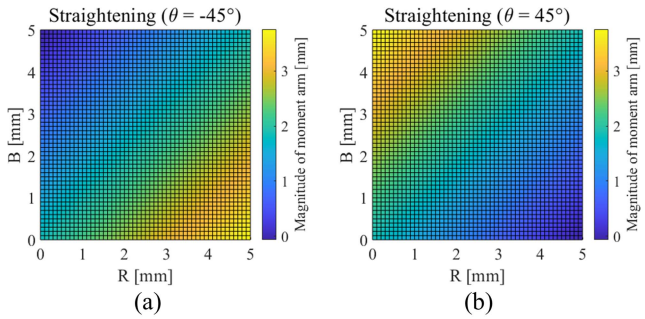

Fig. 6. Change of magnitude of moment arm of the rolling contact joint in dominant direction with respect to the change in *R* and *B*. (a) Straightening phase. (b) Bending phase.

(blue solid line). As calculated from (2), the moment arm of the pulley joint (dashed line) is constant at 2 mm, regardless of the bending angle. For the pin joint (dashed and dotted lines), the moment arm was less than 2 mm during the straightening phase and greater than 2 mm during the bending phase. This result implies that the pin joint is advantageous for the bending phase; however, it is disadvantageous for the straightening phase in terms of the moment arm. For the rolling contact joint, the slope of the moment arm was affected by the difference between the *R* and *B*.

A rolling contact joint should be designed such that it exhibits a large magnitude of the moment arm in the dominant direction during both the straightening and bending phases in terms of *R* and *B*. The moment arm variation of the rolling contact joint for *R* and *B* during both phases ($-45°$ and $45°$) is presented in Fig. 6 using (6). Here, the yellow regions indicate a relatively larger moment arm than the blue regions. Note that during the straightening phase [see Fig. 6(a)], the moment arm increases as *R* increases and *B* decreases. However, during the bending phase [see Fig. 6(b)], the moment arm increases as *R* decreases and *B* increases. This suggests that if the joint design variables *R* and *B* are determined differently according to both phases during bending in the dominant direction, a properly designed rolling contact joint may exhibit a high payload capability in the dominant direction regardless of straightening or bending.

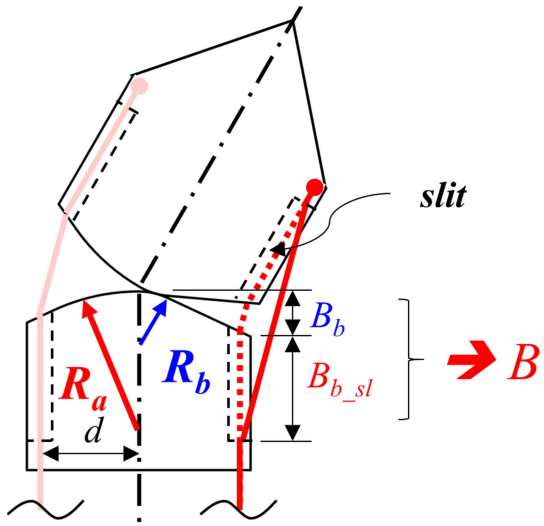

Fig. 7. Kinematic structure of an ARC joint.

B. Payload Analysis of ARC Joint

The kinematic structure of the proposed ARC joint is illustrated in Fig. 7. An obvious difference of this system from the conventional rolling contact joint is that the proposed ARC joint has two different radii of the rolling surface, R_a and R_b. The value of R_a is relatively larger than that of R_b. In addition, this ARC joint had a wire hole with a slit. Owing to this slit, the height of the wire hole changes as the sign of the bending angle changes, and the actuating wire path changes from the red dotted line to a red solid line. Therefore, the magnitude of the moment arm of the ARC joint on the right-hand side increases. The magnitudes of the moment arms of the ARC joint on the left- (m_a) and right- (m_b) hand sides differ from that of the conventional rolling contact joint. During the straightening phase ($\theta < 0$), the two moment arms m_a and m_b are calculated as

$$m_a(\theta) = d\cos\frac{\theta}{2} + (R_a - B_a - B_{a\_sl})\sin\frac{\theta}{2} \tag{7}$$

$$m_b(\theta) = d\cos\frac{\theta}{2} - (R_a - B_b)\sin\frac{\theta}{2} \tag{8}$$

where B_{a_sl} is the height of the slit on the left-hand side. In this phase, a large R_a makes m_a large; therefore, the payload can be higher than that achieved when R_a is small. The height of the slit does not affect the payload. During the bending phase ($\theta \geq 0$), m_a and m_b are calculated as

$$m_a(\theta) = d\cos\frac{\theta}{2} + (R_b - B_a)\sin\frac{\theta}{2} \tag{9}$$

$$m_b(\theta) = d\cos\frac{\theta}{2} - (R_b - B_b - B_{b\_sl})\sin\frac{\theta}{2} \tag{10}$$

where B_{b_sl} is the height of the slit on the right-hand side. In this phase, a small R_b makes m_b larger. In addition, the height of the slit increases, as shown by the red line in Fig. 7. Therefore, the payload can be increased during both the straightening and

TABLE I
SUMMARIZED RESULTS OF THE PAYLOAD IN THE DOMINANT DIRECTION DEPENDING ON THE JOINT TYPE

Joint type	Pin (R=0)	Symmetric rolling (R=1.5)	Symmetric rolling (R=4.5)	Symmetric rolling with slit (R=4.5, B_{sl}=2)	Pulley	Asymmetric rolling (R_a=4.5, R_b=1.5, B_{b_sl}l=0)	Asymmetric rolling with slit (R_a=4.5, R_b=1.5, B_{b_sl}=2)
Average length of the moment arm [mm] (Max. length)	1.94 (2.87)	1.94 (2.24)	1.94 (2.66)	2.15 (2.66)	2.00 (2.00)	**2.26** (2.66)	**2.47** (3.08)
Ratio of increase [%]	-	-	-	11.0	3.3	**16.6**	**27.5**

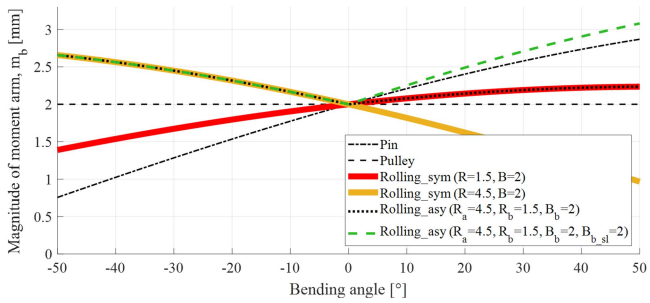

Fig. 8. Comparison of the magnitudes of moment arms in the dominant direction. Dashed line = pulley joint; dashed and dotted line = pin joint; red solid line = symmetric rolling contact joint with R = 1.5 mm; orange solid line = symmetric rolling contact joint with R = 4.5 mm; blue dotted line = proposed ARC joint with R_a = 4.5 mm and R_b = 1.5 mm; green dashed line = proposed ARC joint with a wire hole slit.

bending phases by utilizing an asymmetric rolling surface and wire hole with a slit.

Fig. 8 shows the simulation results of the moment arm variation of the proposed ARC joint with R_a = 4.5 mm and R_b = 1.5 mm in the dominant direction. The magnitude of the moment arm of the proposed ARC joint followed that of the symmetric rolling contact joint with an R value of 4.5 mm during the straightening phase ($\theta < 0$). After passing through 0°, the magnitude of the moment arm of the ARC joint followed that of the symmetric rolling contact joint with an R value of 1.5 mm during the bending phase ($\theta \geq 0$). Notably, during both phases, the ARC joint exhibits the advantages of both a large radius of the rolling surface during the straightening phase and a small radius of the rolling surface during the bending phase. In addition, as B_{b_sl} increased, the magnitude of the moment arm in the dominant direction during the bending phase increased. However, the magnitude of the moment arm during the straightening phase did not change because the slit did not affect the actuating wire path.

To quantitatively compare the payload among the abovementioned joints, the average length of the moment arm for each joint was calculated for bending angles of −50° and 50° (see Table I). The results suggest that a long length corresponds to a higher payload capability than achieved with a short length within the bending phase. The ratio of increase was calculated based on the moment at which the area of the pin joint was zero. Notably, regardless of the radius of the rolling surface of the rolling contact joint, the average length of the moment arm was constant at 1.94 mm. In addition, as shown in Fig. 5, the magnitude of the moment arm of the symmetric rolling contact joint decreased in the straightening phase and increased in the bending phase as the radius of the rolling surface decreased. The pin joint, which can be regarded as a symmetric rolling contact joint with a radius of zero on the rolling surface, had the same average value as that of the moment arm. For the pulley joint, the length of the moment arm was constant regardless of the bending angle, and the average length of the moment arm increased by 3.3%.

However, the proposed ARC joint exhibited a higher payload capability than other investigated joints. The length of the moment arm of the ARC joint without a slit increased by 16.6% compared to those of the pin and symmetric rolling contact joints and by 12.9% compared to the pulley joint. For the ARC joint with a slit, the length of the moment arm increased by 27.5% compared to the pin and symmetric rolling contact joints, and it increased by 23.5% compared to the pulley joint. Conversely, the payload in the nondominant direction decreased, as expected. For the ARC joint without a slit, the payload decreased by 17.0% compared with the symmetric rolling contact joint. For the ARC joint with the wire hole slit, the payload decreased by only 0.06%. These results indicate that even though the payload of the ARC joint in the nondominant direction is smaller, it is comparable to that of the conventional rolling contact joint. Therefore, it was confirmed that the proposed ARC joint had a higher payload capability than other conventional joints.

C. Design Constraints of the ARC Joint

In this section, the design constraints of the ARC joint with diameter of 3.4 mm are determined. The goal is to design a flexible instrument with an ARC joint that is suitable for ESD and general suturing tasks. Although various studies have been conducted considering the design parameters of rolling contact joints [29], [30], [31], only symmetric rolling contact joints have been investigated. Because the ARC joint has two different radii, R_a and R_b should also be determined as design constraints (DCs). The following DCs were set:

1) DC 1. Higher payload in dominant direction: To generate a higher payload in the dominant direction, R_a should be larger than R_b

$$R_a > R_b. \tag{11}$$

2) DC 2. Minimum number of joints for one bending process: As the number of joints increases, the stiffness of the underactuated manipulator decreases [31]. Therefore, the number of joints should be small. However, in a single joint for one bending process, the excessive bending of the wire occurs, which causes high friction between the wire and link and results in wire

wear or permanent deformation. Considering these effects, the minimum number of joints (n) required for one bending process was determined to be two

$$n \geq 2. \tag{12}$$

3) DC 3. Stack sequence of joint for bending DOFs: For the ESD task, surgical instruments should be accessible regardless of the direction of the lesion and should be capable of grasping and lifting the mucosa layer in the desired direction. Therefore, for the ESD task, the minimum bending DOF was 2. Meanwhile, the basic motions of the suturing task comprise reach, orientation, push, and pull [32]. Among them, the reach motion requires a bending motion of the instrument with two DOFs. Therefore, the minimum bending DOF for ESD and general suturing was 2. The number of joints required for two bending DOFs (pitch and yaw) was determined based on research on the joint stack sequence [33]. It was found that for a two-DOF discrete bending joint, the $2n$+1 unit can perfectly transmit a proximal axial rotation to the distal tip. Therefore, the stack sequence was determined as Y-P-Y-P-Y from the proximal side, where Y and P are the yaw and pitch, respectively.

4) DC 4. Maximum bending angle of entire instrument: The range of motion changes $\theta_{req.\max}$ according to the size of R. Using a simple trigonometric calculation for the radius of the rolling surface, the following equation was derived:

$$2n\sin^{-1}\left(\frac{d}{R}\right) \geq \theta_{req.\,\max}. \tag{13}$$

In this study, $\theta_{req.\max}$ was set to be 100° using plane. The d, the distance between the wire hole and central axis of the link should be large to achieve a high payload within the mechanical limits of the link, as can be seen in (8) and (10). As this distance increases, the length between the wire hole and the outer surface of the link shortens, making it very difficult to manufacturing. Therefore, considering the manufacturability of the link and wire hole, distance d was determined to be 1.25 mm. Meanwhile, the minimum bending angle occurs when the number of joints is small and the radius of the rolling surface is large. When $\theta_{req.\max}$ is 100°, d is 1.25 mm, and n is two, R_a and R_b should satisfy the following inequality:

$$0 < R_b < R_a \leq 2.95. \tag{14}$$

5) DC 5. Minimum radius of bending curvature: Considering the two-DOF bending joint, the radius of the bending curvature can be calculated as

$$\frac{H\cos\frac{\theta_{req.\,\max}}{2n} + R\left(1-\cos\frac{\theta_{req.\,\max}}{2n}\right)}{\sin\frac{\theta_{req.\,\max}}{2n}} \leq \rho_{req.\,\min} \tag{15}$$

where H and $\theta_{req.\max}$ are the length of the link and maximum bending angle of the entire instrument, respectively. The bending curvature of the ARC joint varies according to the size of R. The worst case in terms of the radius of bending curvature occurs when n and R are large such that complete bending occurs. When $\rho_{req.\min}$ is 10 mm, n is 3, and R is 2.9 mm, as obtained above, the link length H may then be determined as

$$H \leq 2.86. \tag{16}$$

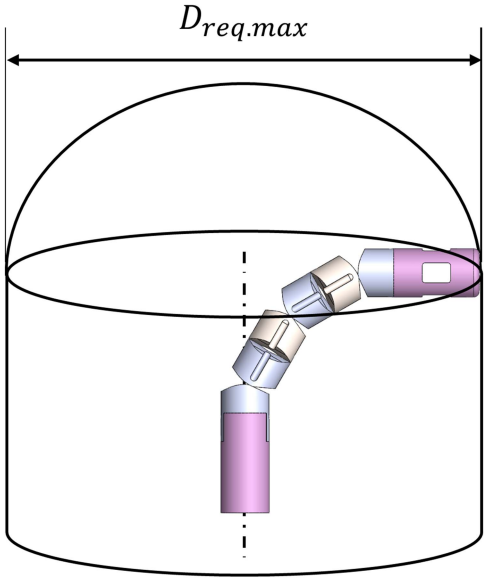

Fig. 9. Cylindrical shape of the flexible instrument.

6) DC 6. Maximum workspace of instrument: For the two-DOF bending instrument, the workspace had a cylindrical shape (see Fig. 9). The workspace of the instrument can be expressed as

$$(2H_e - R_a - R_b)\sin\theta + 2(R_a + R_b)\sum_{i=1}^{n}\sin\frac{2i-1}{2n}\theta + 2(2H - R_a - R_b)\sum_{i=1}^{n}\sin\left(\frac{2(i-1)}{2n}\theta\right) \geq D_{req.\,\max} \tag{17}$$

where H_e is the length of the end tip of the instrument, such as a cautery knife or grasper. If R_a and R_b are combined on the left-hand side and rearranged, (17) can be written as

$$R_a + R_b \geq \frac{4H\sum_{i=1}^{n}\sin\frac{2(i-1)}{2n}\theta + 2H_e\sin\theta - D_{req.\,\max}}{\sin\theta - 2\sum_{i=1}^{n}\sin\frac{2i-1}{2n}\theta + 2\sum_{i=1}^{n}\sin\frac{2(i-1)}{2n}\theta}. \tag{18}$$

Considering early-stage tumors that exhibit an average diameter of approximately 30 mm [34], it is necessary to have a workspace larger than the size of the lesion to perform the entire ESD process using only the surgical instrument without the movement of the overtube. Therefore, under conservative conditions that exclude the movement of the overtube, the workspace of the surgical instrument must be able to access a circular area with a radius of approximately 30 mm or more in front of the endoscope. R_a and R_b should be therefore determined by considering this circular area.

7) DC 7. Minimum magnitude of moment arm: Because of the asymmetric shape of the proposed joint's rolling surface, it has a lower magnitude of the moment arm in the nondominant direction compared to that in the dominant direction. The moment arm in the nondominant direction should be positive for bending motions conducted over the entire bending range. Moreover, d

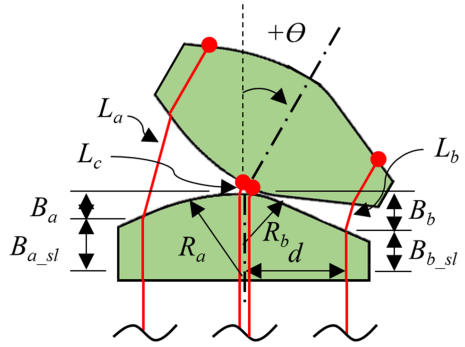

Fig. 10. Kinematic structure of the ARC joint for calculating the wire length between nearby links.

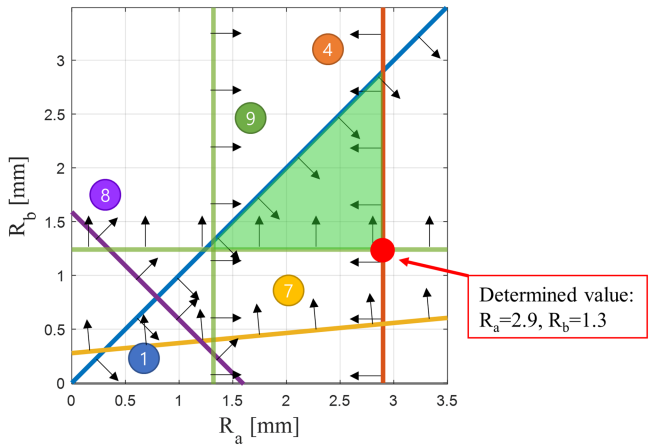

Fig. 11. Feasible regions for the design parameter for R_a and R_b.

is a criterion used to determine the minimum magnitude of the moment arm because it relates to the magnitude of the moment arm achieved when the instrument is in a neutral position. The magnitude of the moment arm in the nondominant direction during the bending phase can be expressed using the criterion d as follows:

$$m_a = d\cos\frac{\theta_{req.\max}}{2} + (R_b - B_a)\sin\frac{\theta_{req.\max}}{2} \geq d \quad (19)$$

where $\theta_{req.\max}$ is the maximum bending angle of a single joint. Using a simple trigonometric calculation, the height of the wire hole B_a can be calculated as follows:

$$B_a = R_a\left(1-\cos\frac{\theta_{req.\max}}{2}\right) + \left(d - R_a\sin\frac{\theta_{req.\max}}{2}\right)\tan\frac{\theta_{req.\max}}{2}. \quad (20)$$

When d is 1.25 and $\theta_{req.\max}$ is 50°, by substituting (20) into (19), the following constraint can be obtained:

$$R_b \geq 0.094R_a + 0.277. \quad (21)$$

The magnitude of the moment arm in the nondominant direction during the straightening phase was not considered because we aim to design a joint with a high payload in the dominant direction. If the magnitude of the moment arm in the nondominant during the straightening phase is larger than d, R_b should be much larger than R_a. However, this did not correspond to the purpose of the study.

8) DC 8. Avoiding slack in wire: Wire slack during the bending motion degrades the positional accuracy of the instrument. It occurs when the change in the length of the actuating wire required to drive the joint is less than zero. At this time, the change in the wire driving the other joints is not considered. For example, to calculate the slack in the pitch joint, only the actuating wire for the driving pitch joint is considered. As shown in Fig. 10, the wire lengths and total change in the wire were calculated differently based on the sign of the bending angle. When the bending angle is less than 0°, the calculation results may be expressed as

$$L_a(\theta) = 2\left(R_a - (R_a - B_a - B_{a\_sl})\cos\frac{\theta}{2} + d\sin\frac{\theta}{2}\right)$$

$$L_b(\theta) = 2\left(R_a - (R_a - B_b)\cos\frac{\theta}{2} - d\sin\frac{\theta}{2}\right)$$

$$\Delta L_{asy\_n}(\theta) = 2(2R_a - B_a - B_b - B_{a\_sl})\left(1-\cos\frac{\theta}{2}\right) \quad (22)$$

where L_a, L_b, and $\Delta L_{asy\_n}(\theta)$ are the wire length on the left-hand side, wire length on the right-hand side, and total change in the wire length of the ARC joint with a negative bending angle, respectively. When the bending angle is greater than 0°, the calculation results may be expressed as

$$L_a(\theta) = 2\left(R_b - (R_b - B_a)\cos\frac{\theta}{2} + d\sin\frac{\theta}{2}\right)$$

$$L_b(\theta) = 2\left(R_b - (R_b - B_b - B_{b\_sl})\cos\frac{\theta}{2} - d\sin\frac{\theta}{2}\right)$$

$$\Delta L_{asy\_p}(\theta) = 2(2R_b - B_a - B_b - B_{b\_sl})\left(1-\cos\frac{\theta}{2}\right) \quad (23)$$

where $\Delta L_{asy\_p}(\theta)$ is the total change in the wire length of the ARC joints with positive bending angles. Consequently, the constraints for R_a and R_b can be derived as

$$R_a > \frac{1}{2}(B_a + B_b + B_{a\_sl}) = 1.32 \ \ (\theta < 0)$$

$$R_b > \frac{1}{2}(B_a + B_b + B_{b\_sl}) = 1.24 \ \ (\theta > 0). \quad (24)$$

We considered various design constraints. To determine R_a and R_b, the design constraints 1, 4, 7, and 8 are shown in Fig. 11. In this study, the design constraint 6 did not affect the determination of R_a and R_b. If the design constraints change depending on the task environment, design constraint 6 may have an impact. The green area shows the feasible range of R_a and the R_b that satisfies three of these constraints. Because the effect of the payload enhancement in the dominant direction of the ARC joint increases as R_a increases and R_b decreases, the

TABLE II
DETERMINED DESIGN PARAMETERS OF THE INSTRUMENT

Design parameters	R_a	R_b	B_a	B_{a_sl}	B_b	B_{b_sl}	d	H	n_{yaw}	n_{pitch}
Dimension [mm]	2.9	1.3	0.28	1.91	0.45	1.74	1.25	2.8	2 [-]	3 [-]

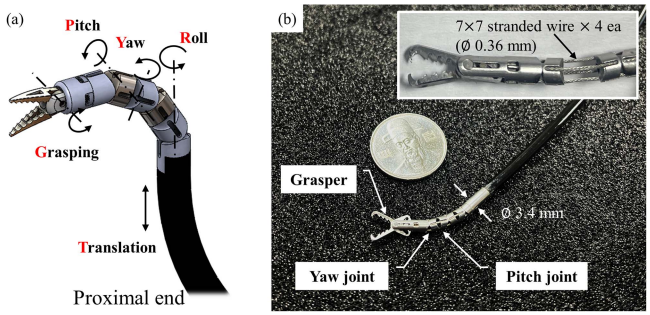

Fig. 12. Surgical instrument utilizing the ARC joint. (a) 3-D CAD model and (b) fabricated instrument with actuating wire configuration.

objective function becomes

$$\arg\min_{R_a,\,R_b} \frac{R_b}{R_a}. \tag{25}$$

Therefore, R_a and R_b were determined as 2.9 mm and 1.3 mm, respectively. In addition, the remaining design parameters of the ARC joint were determined, as listed in Table II.

Applying the above design parameters, a flexible endoscopic surgical instrument with a diameter of 3.4 mm was designed [see Fig. 12(a)]. There are five DOFs in this surgical instrument, which consist of translation, roll, pitch, and yaw from the proximal end, and the grasper as an end-effector. Fig. 12(b) shows the fabricated surgical instrument using the ARC joint. Stainless-steel 304 (SUS 304) was used as the link. For the actuating wire, a 7±7 stranded stainless-steel wire with a diameter of 0.36 mm was used, and the diameter of the wire hole of each link was designed to be 0.5 mm. The National Electrical Code (NEC) recommends a wire-hole-to-wire fill ratio of lower than 53% [35]. In addition, the coil springs were used as a sheath with an outer diameter of 0.8 mm and inner diameter of 0.5 mm.

III. EXPERIMENTS AND RESULTS

A. Payload Experiment

To compare the payload capability of the designed system with that of a conventional joint, a symmetric rolling contact joint was designed with a rolling surface radius of 1.5 mm (see Fig. 13). All design variables except for the radius of the rolling surface were identical. Because the pulley joint always has the same size moment arm regardless of the bending angle, it is obvious that similar experimental results will be obtained even if the payload experiment is conducted. In addition, a pin joint can be considered as a symmetric rolling contact joint with a radius of rolling surface of zero, as explained in Section II. Therefore, the payload experimental result of the pin joint can be predicted in the payload experiment. To ensure that the

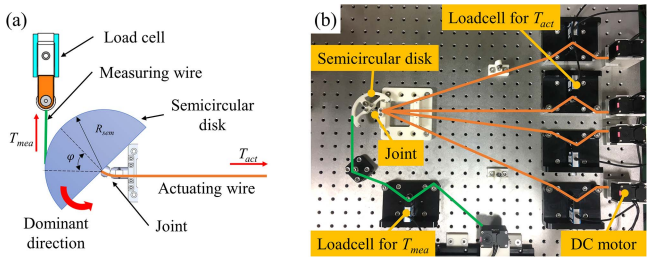

Fig. 13. Experimental setup for measuring the payload. (a) Schematic diagram of payload measurement method. (b) Overview of the experimental setup.

magnitude of the moment arm of the measuring wire was nearly constant regardless of the bending angle of the bending joint, a semicircular disk with a radius of 40 mm (R_{sem}), which is considerably larger than the diameter of the joint, was attached to the distal end of the joint. A measuring wire fixed to the end of the semicircular disk was wound around it and fixed to the load cell (T_{mea}) for a green line in Fig. 13(b). Before bending, the joint was placed in a neutral position (0°) and all the actuating wires [orange lines in the Fig. 13(b)] were pulled using dc motors by a pretension force of 5 N. The measuring wire was pulled using a dc motor until it moved. The tension of the actuating wire (T_{act}) and the tension of the measuring wire were measured using the load cells while bending the joint in the dominant direction with the actuating wire. The payload experiment was repeated five times for each angular condition and the payload data were obtained as the average value of the measured tension. We used five motors of Dynamixel XM-430 (ROBOTIS Ins., South Korea). Four motors were used for winding and releasing the actuating wires and one motor was used for winding the measuring wire. Five load cells of 333FDX (KTOYO co., Ltd, South Korea) were used to measure the tension of wires.

Fig. 14 shows the experimental results obtained while increasing the tension of the actuating wire at five bending angles from −40° to 40° at intervals of 20°. The red and black solid lines represent the payloads of the symmetric rolling joint and the proposed ARC joint, respectively. In Fig. 14, the bending angles of −40° and −20° correspond to the straightening phase, while the bending angles of 20° and 40° correspond to the bending phase. Except for the case in which the magnitudes of the moment arms of both joints are equal and the bending angle is 0°, the payload of the ARC joint is always greater than that of the conventional symmetric rolling contact joint in both the straightening and bending phases. The quantitative values of the payload are summarized in Table III. When the bending angle was −40° and T_{act} was 60 N, T_{mea} for the symmetric rolling contact and ARC joints were 1.69 N and 2.62 N, respectively. The T_{mea} value of the ARC joint was enhanced by 55.0% compared with that of the symmetric rolling contact joint. Similarly, when the bending angles were −20°, 20°, and 40°, the payload of the ARC joint was enhanced by 26.0%, 40.1%, and 71.9% respectively, compared to the symmetric rolling contact joint. In this payload experiment, we compared the payload to the symmetric rolling contact joint with a radius of 1.5 mm as a

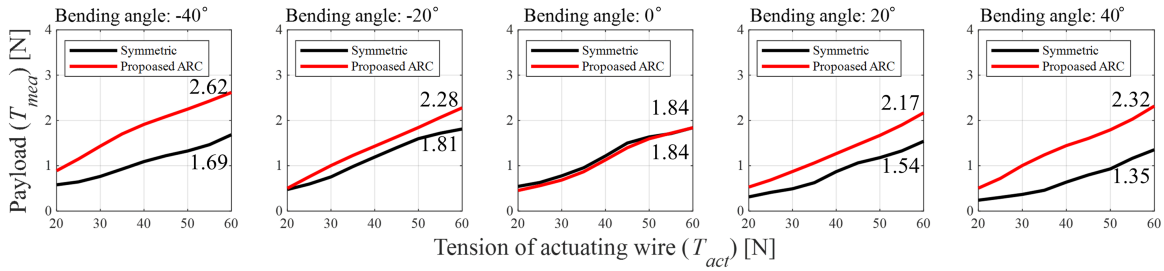

Fig. 14. Experimental results of payload of the surgical instrument with the ARC joint with a diameter of 3.4 mm. Red and black solid lines represent the conventional symmetric rolling contact joint and the proposed ARC joint, respectively. Bending angle: (a)−40°, (b) −20°, (c) 0°, (d) 20°, and (e) 40°.

TABLE III
PAYLOAD OF THE JOINT AT A TENSION OF 60 N

Bending angle [°]	-40		-20		0		20		40	
Joint type	Sym	ARC	Sym	ARC	Sym	ARC	Sym	ARC	Sym	ARC
Payload [N]	1.69	2.62	1.81	2.28	1.84	1.84	1.54	2.17	1.35	2.32
Ratio of increase [%]	55.0		26.0		0.0		40.1		71.9	

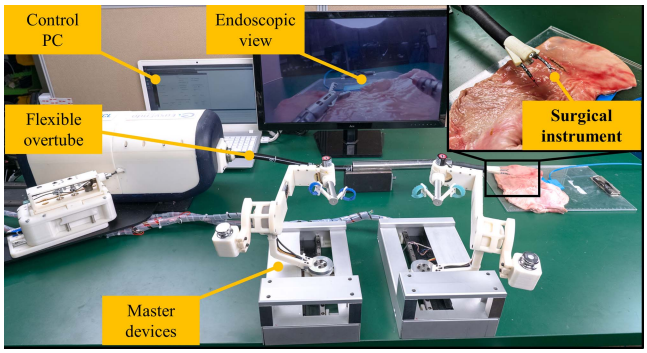

Fig. 15. Experimental setting for ex vivo surgical tasks.

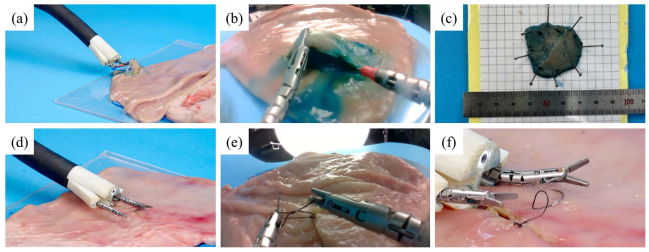

Fig. 16. Experimental procedure and results. (a) ESD task, (b) endoscopic view of the ESD task, (c) dissected specimen, (d) suturing task, (e) endoscopic view for suturing, and (f) completed knot.

comparison target. The ratio of increase could vary depending on the radius of the symmetric rolling contact joint.

B. Ex Vivo Trials: ESD and Suturing

To verify the endoscopic surgical performance of the proposed ARC joint, preliminary ex vivo experiments were performed for ESD and general suturing tasks on an extracted porcine stomach (see the supplementary video). Grasping forceps and needle drivers with the proposed ARC joint were used as surgical instruments for the ESD and suturing tasks, respectively. Fig. 15 shows the experimental setup for the ex vivo experiments. K-FLEX [23], a flexible endoscopic surgical platform that was developed by our research team, was used as a flexible channel to introduce the flexible instruments into the surgical site. Ergonomic and intuitive master devices with redundant joints [36] that were also developed by our research team were used to operate the surgical instruments. The operator manipulated the master devices while watching the endoscopic video, which was displayed from the camera fixed at the end of the overtube.

Fig. 16(a)–(c) shows the complete ESD procedure. The operator manipulated the hook cautery using the rightmost master device and grasping forceps with the leftmost master device. They manipulated the master devices to mark the lesion location (marking), inject the solution (injection), precut the mucosa layer around lesion (precut), dissect the mucosa with a hook cautery (dissection), and lift the flap of the mucosal layer with the grasping forceps. Using the grasping forceps with the proposed ARC joint, the operator can effectively lift the flap of the mucosal layer to expose the dissection plane and produce the endoscopic view [see Fig. 16(b)]. The ESD task was performed without perforation. The entire procedure took approximately 635 s and the procedure speed was 1.47 mm^2/s (dissected area: 934.6 mm^2).

In addition, the suturing task was performed with two needle drivers comprising the ARC joint [see Fig. 16(d)–(f)]. In this suturing task, a simple interrupted suture, a popular suturing method, was used as the stitching procedure. The operator pierced the mucosal layer with the rightmost needle driver while holding the mucosal layer with the leftmost needle driver. After stitching, knot tying was performed by making two loops and pulling the thread on both sides. Fig. 16(f) shows that the incision was completely sutured using two needle drivers. The entire procedure took approximately 8 min, with 5 min for stitching and 3 min for knot tying. Furthermore, to verify the safety of

suturing performed using the proposed instrument with the ARC joint, the tension of the thread after knot-tying was measured. The force for tissue damage was previously reported to be 1.5 N [37]. We found that the completed knot was not released or broken until a thread tension of 6.2 N, was enacted, indicating a secure suture.

IV. Discussion

Payload experimental results show that the proposed ARC joint has significantly enhanced payload capability in dominant direction compared to the conventional symmetric rolling contact joint. Furthermore, the difference in payload between the symmetric rolling contact joints and the ARC joint also increased as the absolute value of bending angle of the joint increased. In particular, the rate of payload increases in bending phase was higher than that of increase in straightening phase with the effect of the slit of wire hole. This payload characteristics of the ARC joint is advantageous when lifting the mucosa upward. Because of the elastic behavior of mucosa, the stress increases as it is stretched by tension [38]. Therefore, a higher force is required as the mucosa is stretched. Similarly, it is helpful for knot-tying because the payload increases as the bending angle of the surgical instrument increases during pulling the thread outward. In addition, ex vivo tests for ESD and general suturing tasks were performed to verify the endoscopic surgical performance of this system. Using grasping forceps, the operator could effectively lift the flap of the mucosal layer to expose the dissection plane during an ESD task and it allowed operator to dissect the mucosal layer easily. In a previous study [39], we performed the ESD task from precut to dissection using a symmetric rolling contact joint. Although the entire procedure speed (from marking to dissection) was not measured, the procedure speed for precut and dissection were 2.37 mm^2/s and 1.69 mm^2/s, respectively. In this study, using the proposed ARC joint, the procedure speed for precut and dissection were 12.5 mm^2/s and 2.1 mm^2/s, respectively. Thus, a faster ESD task is possible when using the proposed ARC joint. Also, a suturing task was successfully completed with the proposed ARC joint. Secure operation was possible not only in looping motion (requiring dexterity of surgical instruments) but also in knot-tying (requiring high payload capability).

The greatest advantage of the proposed joint is its extendibility. The joint was designed based on a conventional symmetric rolling contact joint. Therefore, wherever a symmetric rolling contact joint is used, this joint can be applied and used to exert a high payload. For the same reason, depending on the joint stack sequence, 1-DOF bending or 2-DOF bending motion can be easily realized. In addition, this joint can be easily designed in a variety of sizes (even less than 3.4 mm) depending on the usage environment and required amount of payload. Above all, the enhanced payload capability of this joint in the dominant direction may be useful for cable-driven instruments composed of single or multiple joints that require a high payload in a specific direction.

In summary, the ARC joint, compared to previous studies with symmetric joints, enables a 2-DOF bending motion and can be realized in the same size as the symmetric joint. However, it possesses a higher payload capability in the dominant direction and it demonstrated superior performance in surgical tasks in terms of process speed.

V. Conclusion

In this study, an ARC joint was proposed to overcome the limitations of conventional flexible endoscopic instruments with low payload capabilities. To generate a high payload in the dominant direction within the limited size of the flexible instrument, the ARC joint was designed to have two different radii for the rolling surface and wire hole with a slit. The payload at a single ARC joint was calculated, confirming its higher payload capability in the dominant direction compared to other conventional joints, pulleys, pins, and rolling joints. Subsequently, the design constraints were determined, and the design parameters were set. An experimental evaluation of the system was performed using a surgical instrument, and it was verified that the proposed ARC joint can lift enhanced payloads compared to those observed using the conventional symmetric rolling contact joint. To verify the feasibility for the endoscopic surgical performance, ex vivo tests for ESD and general suturing tasks were also performed and the proposed ARC joint successfully completed these tasks.

In future, stiffness analysis is required as the joint's stiffness under an external force is an important factor in designing a flexible instrument. Stiffness is affected by the stiffness of the actuating wire, number of joints, and length and pretension of the actuating wire. In addition, the hysteresis of the ARC joint should be investigated. Unlike the conventional symmetric joints, the proposed ARC joint is expected to exhibit asymmetrical hysteresis behavior because the lengths and tensions of the wire required for bending in the dominant and nondominant directions differ. This asymmetric hysteresis degrades the positional accuracy in both the directions and it is a challenge to compensate for this hysteresis. One of the possible ways to compensate for the asymmetric hysteresis is to use two actuators for one bending DOF while pushing or releasing actuating wires. Asymmetric hysteresis could be reduced if two actuators are controlled by two different wire lengths required for joint bending. Although the subject in this study followed the expert's surgical guide during the ex vivo test, verification with experts will be carried out to rigorously compare the surgical performance of the proposed surgical instrument with that of a conventional flexible endoscope.

References

[1] F. Bray, J. Ferlay, I. Soerjomataram, R. L. Siegel, L. A. Torre, and A. Jemal, "Global Cancer Statistics 2018: Globocan estimates of incidence and mortality worldwide for 36 cancers in 185 countries," *Cancer J. Clin.*, vol. 68, no. 6, pp. 394–424, 2018.

[2] T. Gotoda, "Endoscopic resection of early gastric cancer," *Gastric Cancer*, vol. 10, pp. 1–11, 2007.

[3] M. Noda et al., "Possibilities and limitations of endoscopic resection for early gastric cancer," *Endoscopy*, vol. 29, no. 05, pp. 361–365, 1997.

[4] T. Oyama, "Counter traction makes endoscopic submucosal dissection easier," *Clin. Endoscopy*, vol. 45, no. 4, 2012, Art. no. 375.

[5] N. Fukami, "What we want for ESD is a second hand! traction method," *Gastrointestinal Endoscopy*, vol. 78, no. 2, pp. 274–276, 2013.

[6] I. Saito et al., "Complications related to gastric endoscopic submucosal dissection and their managements," *Clin. Endoscopy*, vol. 47, no. 5, 2014, Art. no. 398.
[7] N. E. Conway and L. L. Swanström, "Endoluminal flexible endoscopic suturing for minimally invasive therapies," *Gastrointestinal Endoscopy*, vol. 81, no. 2, pp. 262–269, 2015.
[8] S. N. Stavropoulos, R. Modayil, and D. Friedel, "Current applications of endoscopic suturing," *World J. Gastrointestinal Endoscopy*, vol. 7, no. 8, 2015, Art. no. 777.
[9] P. W. Chiu et al., "Closure of a gastrotomy after transgastric tubal ligation by using the eagle claw vii: A survival experiment in a porcine model (with video)," *Gastrointestinal Endoscopy*, vol. 68, no. 3, pp. 554–559, 2008.
[10] I. Schiefke, A. Zabel-Langhennig, S. Neumann, J. Feisthammel, J. Moessner, and K. Caca, "Long term failure of endoscopic gastroplication (endocinch)," *Gut*, vol. 54, no. 6, pp. 752–758, 2005.
[11] A. Kirschniak, N. Subotova, D. Zieker, A. Königsrainer, and T. Kratt, "The over-the-scope clip (OTSC) for the treatment of gastrointestinal bleeding, perforations, and fistulas," *Surg. Endoscopy*, vol. 25, no. 9, pp. 2901–2905, 2011.
[12] D. J. Abbott, C. Becke, R. I. Rothstein, and W. J. Peine, "Design of an endoluminal NOTES robotic system," in *Proc. IEEE/RSJ Int. Conf. Intell. Robots Syst.*, 2007, pp. 410–416.
[13] Z. Sun, R. Y. Ang, E. W. Lim, Z. Wang, K. Y. Ho, and S. J. Phee, "Enhancement of a master-slave robotic system for natural orifice transluminal endoscopic surgery," *Ann. Acad. Med.- Singap.*, vol. 40, no. 5, 2011, Art. no. 223.
[14] D. Lomanto, S. Wijerathne, L. K. Y. Ho, and L. S. J. Phee, "Flexible endoscopic robot," *Minimally Invasive Ther., Allied Technol.*, vol. 24, no. 1, pp. 37–44, 2015.
[15] P. W. Y. Chiu, K. Y. Ho, and S. J. Phee, "Colonic endoscopic submucosal dissection using a novel robotic system (with video)," *Gastrointestinal Endoscopy*, vol. 93, no. 5, pp. 1172–1177, 2021.
[16] P. J. Johnson et al., "Demonstration of transoral surgery in cadaveric specimens with the medrobotics flex system," *Laryngoscope*, vol. 123, no. 5, pp. 1168–1172, 2013.
[17] D. T. Friedrich et al., "Potential advantages of a single-port, operator-controlled flexible endoscope system for transoral surgery of the larynx," *Ann. Otol. Rhinol., Laryngol.*, vol. 124, no. 8, pp. 655–662, 2015.
[18] P. Berthet-Rayne et al., "The i2snake robotic platform for endoscopic surgery," *Ann. Biomed. Eng.*, vol. 46, no. 10, pp. 1663–1675, 2018.
[19] P. Wisanuvej et al., "Master manipulator designed for highly articulated robotic instruments in single access surgery," in *Proc. IEEE/RSJ Int. Conf. Intell. Robots Syst.*, 2017, pp. 209–214.
[20] F. Nageotte, L. Zorn, P. Zanne, and M. De Mathelin, "STRAS: A modular and flexible telemanipulated robotic device for intraluminal surgery," in *Handbook of Robotic and Image-Guided Surgery*. New York, NY, USA: Elsevier, 2020, pp. 123–146.
[21] L. Zorn et al., "A novel telemanipulated robotic assistant for surgical endoscopy: Preclinical application to ESD," *IEEE Trans. Biomed. Eng.*, vol. 65, no. 4, pp. 797–808, Apr. 2017.
[22] R. Nakadate et al., "Surgical robot for intraluminal access: An ex vivo feasibility study," *Cyborg Bionic Syst.*, vol. 2020, 2020, Art. no. 8378025.
[23] M. Hwang and D.-S. Kwon, "K-flex: A flexible robotic platform for scar-free endoscopic surgery," *Int. J. Med. Robot. Comput. Assist. Surg.*, vol. 16, no. 2, 2020, Art. no. e2078.
[24] M. F. Traeger et al., "Forces in minimally invasive surgery: Reliable manipulation of gastric mucosa and the sigmoid colon," in *Proc. IEEE Int. Conf. Robot. Biomimetics*, 2014, pp. 408–412.
[25] C. D. Klink et al., "Tension of knotted surgical sutures shows tissue specific rapid loss in a rodent model," *BMC Surg.*, vol. 11, no. 1, pp. 1–9, 2011.
[26] J. Oguma et al., "Knot-tying force during suturing and wound healing in the gastrointestinal tract," *J. Surg. Res.*, vol. 140, no. 1, pp. 129–134, 2007.
[27] H. Choi, H.-S. Kwak, Y.-A. Lim, and H.-J. Kim, "Surgical robot for single-incision laparoscopic surgery," *IEEE Trans. Biomed. Eng.*, vol. 61, no. 9, pp. 2458–2466, Sep. 2014.
[28] M. Hwang et al., "A single port surgical robot system with novel elbow joint mechanism for high force transmission," *Int. J. Med. Robot. Comput. Assist. Surg.*, vol. 13, no. 4, 2017, Art. no. e1808.
[29] M. Hwang and D.-S. Kwon, "Strong continuum manipulator for flexible endoscopic surgery," *IEEE/ASME Trans. Mechatron.*, vol. 24, no. 5, pp. 2193–2203, Oct. 2019.
[30] J.-W. Suh, K.-Y. Kim, J.-W. Jeong, and J.-J. Lee, "Design considerations for a hyper-redundant pulleyless rolling joint with elastic fixtures," *IEEE/ASME Trans. Mechatron.*, vol. 20, no. 6, pp. 2841–2852, Dec. 2015.
[31] Y.-J. Kim, S. Cheng, S. Kim, and K. Iagnemma, "A stiffness-adjustable hyperredundant manipulator using a variable neutral-line mechanism for minimally invasive surgery," *IEEE Trans. Robot.*, vol. 30, no. 2, pp. 382–395, Apr. 2014.
[32] C. Cao et al., "Task and motion analyses in endoscopic surgery," in *Proc. ASME Dyn. Syst. Control Division*, 1996, pp. 583–590.
[33] J. Suh, "Utilization of 2 n 1 units for 2-dof discrete bending joint to transmit perfect axial rotation for laparoscopic instruments," *Int. J. Control, Autom. Syst.*, vol. 18, no. 1, pp. 186–195, 2020.
[34] N. Yahagi et al., "Endoscopic submucosal dissection for early gastric cancer using the tip of an electrosurgical snare (thin type)," *Dig. Endoscopy*, vol. 16, no. 1, pp. 34–38, 2004.
[35] National Fire Protection Association, "Chapter 9 Table," *National Electrical Code*, 2008 ed., NFPA, p. 671, 2007.
[36] J. Ahn, J. Kim, H. Lee, M. Hwang, and D.-S. Kwon, "A highly intuitive and ergonomic redundant joint master device for four-degrees of freedom flexible endoscopic surgery robot," *Int. J. Med. Robot. Comput. Assist. Surg.*, vol. 17, no. 1, pp. 1–14, 2021.
[37] S. P. Rodrigues, T. Horeman, J. Dankelman, J. J. van den Dobbelsteen, and F.-W. Jansen, "Suturing intraabdominal organs: When do we cause tissue damage?," *Surg. Endoscopy*, vol. 26, no. 4, pp. 1005–1009, 2012.
[38] J. Zhao, D. Liao, and H. Gregersen, "Tension and stress in the rat and rabbit stomach are location-and direction-dependent," *Neurogastroenterol. Motility*, vol. 17, no. 3, pp. 388–398, 2005.
[39] J. Kim et al., "Effects of flexible surgery robot on endoscopic procedure: Preliminary bench-top user test," in *Proc. 28th IEEE Int. Conf. Robot Hum. Interactive Commun.*, 2019, pp. 1–6.

Jeongdo Ahn received the B.S. degree in mechatronics engineering from the Korea University of Technology and Education, Cheonan, South Korea, in 2012 and the M.S. and Ph.D. degrees in mechanical engineering from the Korea Advanced Institute of Science and Technology, Daejeon, South Korea, in 2014 and 2022, respectively.

He is currently a Senior Researcher with the Department of Robotics and Mechatronics, Korea Institute of Machinery and Materials. His research interests include tendon-driven mechanism, flexible endoscopic surgery robot, two-wheeled legged robot, and soft-exoskeleton using SMA spring.

Minho Hwang received the B.S., M.S., and Ph.D. degrees in mechanical engineering from Korea Advanced Institute of Science and Technology, Daejeon, South Korea, in 2010, 2012, and 2017, respectively.

From 2019 to 2021, he was a Postdoctoral Research Associate with the Electrical Engineering and Computer Sciences Department, University of California Berkeley, CA, USA. He is currently an Assistant Professor with DGIST. He has a special research interest in surgical robot design, surgical task automation, robot grasping and manipulation, and their application for minimally invasive surgery.

Dukyoo Kong received the B.S., M.S., and Ph.D. degrees in mechanical engineering from the Korea Advanced Institute of Science and Technology, Daejeon, South Korea, in 2014, 2016, and 2022, respectively.

He is currently a Senior Research Engineer with ROEN Surgical Inc. His research interests include microsurgical instrument, tendon-driven mechanism, joint mechanism, and force sensing of surgical robot.

Joonhwan Kim received the B.S. degree in mechanical engineering from Kyushu University, Fukuoka, Japan, in 2012, and the M.S. and Ph.D. degrees in bioengineering from the University of Tokyo, Tokyo, Japan, in 2014 and 2018, respectively.

From 2018 to 2021, he was a Postdoctoral Researcher with Center for Future Medical Robotics and Human-Robot Interaction Research Center, Korea Advanced Institute of Science and Technology (KAIST), Daejeon, South Korea. He is currently a Senior Researcher with ROEN Surgical Inc., Daejeon, Korea, and is in charge of the development and clinical research of flexible surgical robots. His research interests include flexible surgical robots and instrumentation, clinical validation of medical devices, and human–robot interaction.

Dong-Soo Kwon (Senior Member, IEEE) received the B.S. degree from the Department of Mechanical Engineering, Seoul National University, South Korea, in 1980, the M.S. degree from the Department of Mechanical Engineering, Korea Advanced Institute of Science and Technology (KAIST), Daejeon, South Korea, in 1982, and the Ph.D. degree from the Department of Mechanical Engineering, Georgia Institute of Technology, GA, USA, in 1991.

He was a Visiting Professor with the Department of Mechanical Engineering, Georgia Institute of Technology, from 2008 to 2009. From 1991 to 1995, he worked in Telerobotics Section, Oak Ridge National Laboratory, as a Research Staff. He is currently a Professor with the Department of Mechanical Engineering, KAIST and a Representative Member in Asia-Pacifc area of the Administrative Committee (AdCom) of the IEEE Robotics and Automation Society. In addition, he is the CEO of ROEN Surgical Inc., President of Robot Convergence Forum, South Korea, the Chief Director of the Korea Institute of Robot and Convergence. His research interests include medical robotics, human–robot Interaction, telerobotics, and haptics.